nature
immunology

Transcriptional profiling of stroma from inflamed and resting lymph nodes defines immunological hallmarks

Deepali Malhotra[1,2,8], Anne L Fletcher[1,8], Jillian Astarita[1,2], Veronika Lukacs-Kornek[1], Prakriti Tayalia[3], Santiago F Gonzalez[4], Kutlu G Elpek[1], Sook Kyung Chang[5], Konstantin Knoblich[1], Martin E Hemler[1], Michael B Brenner[5,6], Michael C Carroll[4], David J Mooney[3], Shannon J Turley[1,7] & the Immunological Genome Project Consortium[9]

Lymph node stromal cells (LNSCs) closely regulate immunity and self-tolerance, yet key aspects of their biology remain poorly elucidated. Here, comparative transcriptomic analyses of mouse LNSC subsets demonstrated the expression of important immune mediators, growth factors and previously unknown structural components. Pairwise analyses of ligands and cognate receptors across hematopoietic and stromal subsets suggested a complex web of crosstalk. Fibroblastic reticular cells (FRCs) showed enrichment for higher expression of genes relevant to cytokine signaling, relative to their expression in skin and thymic fibroblasts. LNSCs from inflamed lymph nodes upregulated expression of genes encoding chemokines and molecules involved in the acute-phase response and the antigen-processing and antigen-presentation machinery. Poorly studied podoplanin (gp38)-negative CD31$^-$ LNSCs showed similarities to FRCs but lacked expression of interleukin 7 (IL-7) and were identified as myofibroblastic pericytes that expressed integrin α_7. Together our data comprehensively describe the transcriptional characteristics of LNSC subsets.

The Immunological Genome (ImmGen) Project is a multicenter collaborative venture of immunologists and computational biologists that aims to build a comprehensive, publicly accessible database of gene-expression and gene-regulatory networks in the immune system of the mouse. The data generation involves shared, rigorously controlled methodology and analysis pipelines[1]. As part of this collaboration, we have meticulously analyzed the transcriptomes of lymph node stromal cells (LNSCs) under steady-state and inflammatory conditions.

LNSCs are nonhematopoietic cells crucial for the normal functioning of the immune system, yet they are difficult to study and constitute ~1% of lymph node cellularity. Expression of the glycoprotein podoplanin (gp38) and the adhesion molecule CD31 (PECAM-1) distinguishes the following LNSC subsets: gp38$^+$CD31$^-$ fibroblastic reticular cells (FRCs), gp38$^+$CD31$^+$ lymphatic endothelial cells (LECs), gp38$^-$CD31$^+$ blood endothelial cells (BECs) and gp38$^-$CD31$^-$ double-negative cells (DNCs)[2]. LNSCs have distinct roles in orchestrating immune responses, whereas FRCs and LECs also promote tolerance[3–7]. LECs facilitate the entry of antigen-bearing dendritic cells (DCs) and soluble antigens into lymph nodes[3] and control lymphocyte egress[8], whereas BECs form vessels that allow naive lymphocytes to enter lymph nodes through high endothelial venules[3]. Inside the lymph node, FRCs construct and regulate a specialized reticular network of fibers used by lymphocytes and DCs as a scaffold on which to migrate and interact[3]. Ensheathed by FRCs, the reticular network also forms a complex conduit system of microchannels that rapidly conduct chemokines and other small factors (<70 kilodaltons) from the subcapsular sinus to high endothelial venules[9,10]. During infection, the decoration of high endothelial venules with chemokines attracts leukocytes to lymph nodes, which promotes the adaptive immune response[11]. FRCs also secrete survival factors and chemokines that attract T cells and DCs[2,3]. Indeed, DCs in contact with the reticular network can process tissue-derived soluble antigens, which suggests that conduit-borne lymph may be an important source of antigens during early phases of immune responses or for the maintenance of peripheral tolerance[9,12].

Despite their maintenance of naive lymphocytes, regulation of immune responses and orchestration of DC–T cell interactions, relatively little is known about how FRCs, LECs and BECs interact and are regulated in postnatal life. Moreover, FRC-like cells identified in autoinflammatory or cancerous lesions are associated with worsened clinical outcomes[13,14]. Nonetheless, knowledge of the transcriptional identity of FRCs is limited; at present, it is essentially understood to consist of a generic myofibroblastic phenotype with expression of

identified specialized elements such as chemokines. Evidence suggests that FRCs and LECs may also have important roles in tolerance induction, yet their expression of pathogen receptors and antigen-presenting machinery remains almost completely unstudied.

Transcriptomics is a powerful, unbiased starting point for determining a cell's biology and identifying large numbers of new targets for further study, including molecular pathways, surface receptors and secreted factors. So far, transcriptomics has not been used to examine the specialization of multiple stromal cell types. We therefore aimed to create a comprehensive, 'cross-comparable' database of stromal transcriptional profiles.

We examined the transcriptomes of FRCs, LECs, BECs and poorly studied DNCs[2,6,7], identifying and analyzing each subset's unique expression signature. We matched the expression of immune mediators and growth factors to that of cognate receptors on likely hematopoietic and stromal partners. Analysis of steady-state LNSCs also suggested a readiness to respond to inflammatory or infectious triggers, a hypothesis we further explored by profiling LNSCs that we isolated during an immune response. Next, we more fully characterized the molecular makeup of the lymph-node reticular network. We observed substantial differences in the transcriptional profiles of FRCs and their skin and thymic counterparts, which reflected functional specialization. Finally, whereas the lineage, function, localization and identifying surface markers of DNCs were all previously unknown[2,6,7], this in-depth analysis showed that this subset consists largely of contractile, FRC-like pericytes.

RESULTS

Comparative transcriptional distances between LNSC subsets

To obtain transcriptomes for each subset, we sorted FRCs, LECs, BECs and DNCs to high purity from stroma-enriched fractions of lymph nodes from C57BL/6 mice (**Fig. 1a,b** and **Supplementary Fig. 1a,b**). Through the use of profiling and quality-control pipelines of the ImmGen Project[1], we generated gene-expression profiles on microarrays (**Supplementary Notes 1** and **2**). All data analyzed below passed the quality control of the ImmGen Project, with good replicate quality (median inter-replicate coefficient of variation values of 0.086–0.205). We assumed the general ImmGen Project threshold of 120 after normalization to indicate positive expression (at 95% confidence) and included probes in the comparisons only if they were expressed by at least one cell type and showed low variability within populations (Online Methods). Inspection of the data demonstrated expression of the expected markers, and samples lacked expression of common hematopoietic markers (**Fig. 1c** and **Supplementary Fig. 1c,d**).

We examined global relationships among sorted LNSCs by principal component analysis (PCA), based on the 15% of probes with the greatest difference in expression. This mathematical transformation simplifies multidimensional expression data into principal components, each of which accounts for a proportion of total variability (**Fig. 1d**). For each cell type, samples from skin-draining lymph nodes (SLNs) and mesenteric lymph nodes (MLNs) clustered tightly, which reflected conservation of subset-specific genes between these tissues. Along the first two principal components, which accounted for 83.5% of the observed variability, FRCs and DNCs were positioned closer to each other than to either endothelial subset. However, FRCs and DNCs clearly separated along the third principal component, which demonstrated a transcriptionally distinct relationship. These relationships were also evident on matrix plots of population concordance (measured by Pearson's correlation and Euclidean distance; **Fig. 1e** and **Supplementary Fig. 1e**). Hierarchical clustering of probes with differences in expression reinforced relative

transcriptional similarities between FRCs and DNCs and between LECs and BECs[15] (**Fig. 1f**). These data showed that stromal subsets from different locations did not undergo considerable site-specific differentiation and that DNCs shared more transcriptional similarity with FRCs than with LECs or BECs.

Identification of LNSC subset–specific genes and pathways

Next we compared FRCs with BECs and LECs to identify subset-specific transcriptional signatures (**Fig. 2a**). We used a count of probes with a difference in expression of over twofold as a simple metric of transcriptional differences; SLN FRCs differed from SLN BECs and LECs by 2,026 and 1,936 probes, respectively (**Fig. 2a**). These differences were highly conserved in SLNs and MLNs, as shown by the distribution of probes along the diagonal in the plots comparing change in expression.

Probes upregulated in SLN FRCs relative to their expression in one endothelial cell (EC) subset also tended to be upregulated relative to their expression in the other EC subset (>91.3% of probes; **Fig. 2b**), which emphasized the closer developmental relationship between LECs and BECs. In fact, SLN BECs and LECs differed in expression of fewer probes (**Fig. 2c**), and on average these differences were of a magnitude smaller than those between ECs and FRCs. This pattern was also highly conserved in MLNs (**Fig. 2c**).

To better understand how FRCs differed from sorted ECs, we identified 594 FRC-specific probes and 513 EC-specific probes (upregulated in LECs and BECs; delta score (δ) = 1.0 (adjusted change in expression of twofold or more (adjusted 'fold change' (FC) $\geq$ 2)) for at least one comparison, and δ = 0.85 (adjusted FC $\geq$ 1.8) for all other comparisons; $P < 0.05$ for differences in expression value (EV); **Supplementary Tables 1** and **2**). The delta-score module computes adjusted FCs between two populations, minimizing noise by exponentially penalizing FCs for intrapopulation variability.

To identify previously unknown, immunologically relevant genes and pathways associated with these cells, we analyzed signature probe lists by collating genes into functional pathways in the KEGG database (Kyoto Encyclopedia of Genes and Genomes) and ranking those pathways on the basis of statistical overrepresentation with the DAVID bioinformatics database (Database for Annotation, Visualization and Integrated Discovery)[16]. The list of FRC-specific probes showed enrichment for genes encoding molecules involved in interactions between the extracellular matrix (ECM) and receptors, focal adhesion and cytokine–cytokine receptor interactions (**Fig. 2d**). In contrast, the list of EC-specific probes showed enrichment for genes encoding molecules relevant to leukocyte transmigration. That list also showed enrichment for genes encoding molecules involved in signaling via vascular endothelial growth factors (VEGFs) and cell-cell adhesion, vital for the regulation of vessel integrity and permeability (**Fig. 2d**). These global overviews confirmed known stromal functions, which allowed us to simultaneously comb cell-specific lists for genes not reported before in LNSCs while providing clues to the likely function of the molecules they encode.

Molecular communication in the lymph node

We explored the enrichment of FRCs for higher expression of cytokine-related genes by examining LNSC expression of cytokines, growth factors and immunologically relevant receptors, paired with the expression of cognate ligands and receptors by stroma and key hematopoietic populations (**Fig. 3a,b**). We identified LNSCs as rich sources of signals and growth factors recognized by hematopoietic cells (**Fig. 3a,b**). LNSCs shared expression of receptors for common immune mediators such as type I and type II interferons, TGF-β and
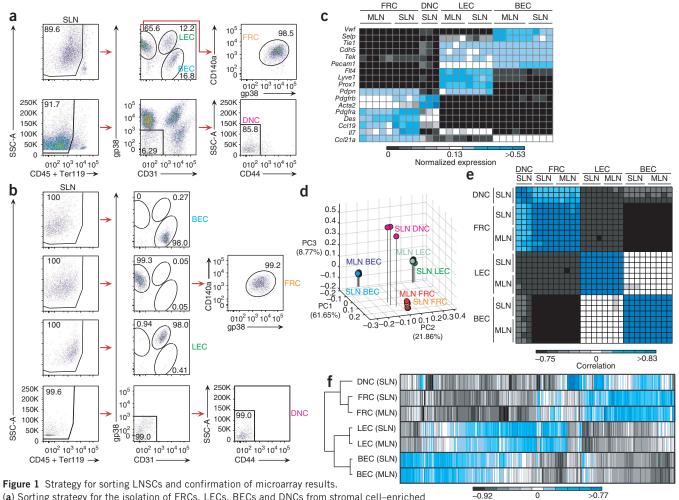
Figure 1 Strategy for sorting LNSCs and confirmation of microarray results.
(**a**) Sorting strategy for the isolation of FRCs, LECs, BECs and DNCs from stromal cell–enriched fractions of pooled SLNs or MLNs. Numbers in or adjacent to outlined areas indicate percent CD45^{−} stroma (left) and each LNSC subset (center and right). SSC, side scatter. (**b**) Analysis of the purity of SLN FRCs, LECs, BECs and DNCs after sorting. Numbers in or adjacent to outlined areas indicate percent cells in each throughout. (**c**) Heat map of hierarchically clustered expression data for genes characteristic of FRCs, LECs or BECs (row-normalized data). (**d**) PCA of LNSC subsets, calculated for the 15% of probes with the greatest difference in expression among LNSC subsets (EV > 120 for any subset), with log$_2$-transformed and row- and column-standardized data. Numbers in parentheses indicate the proportion of total variability accounted for by each principal component (PC1–PC3). (**e**) Heat map of coefficients of correlation for the 15% of probes with the greatest difference in expression among LNSCs (log$_2$-transformed and row-standardized data). Blue indicates the highest correlation. (**f**) Unbiased hierarchical clustering of probes with the greatest difference in expression (EV > 120 for any population, FC > 2 for any pairwise population comparison, and coefficient of variation (CV) < 0.5 within each population), calculated for log$_2$-transformed, row mean-centered and row-normalized data. Data are representative of three to five experiments with 10–30 mice per replicate (**a**), three to five experiments (**b**), one experiment with three to five independent replicates (**c–e**) or one experiment with three to five independent replicates (**f**; mean values).

TNF; however, subsets also showed unique transcriptional profiles for cytokine and chemokine responsiveness, pathogen recognition, and costimulatory potential (**Fig. 3a,b** and **Supplementary Fig. 2a,b**).
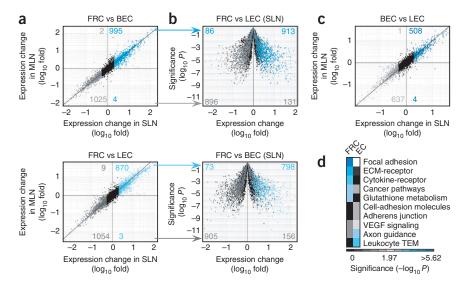
Interleukin 7 (IL-7) crucially maintains naive lymphocytes in lymph nodes[2,3], and although IL-7 mRNA has been found in FRCs, 10% as much transcript has also been detected in pooled ECs[2]. We found that FRCs and LECs produced IL-7 transcripts, whereas BECs and DNCs did not (**Fig. 3a**). Furthermore, T cells, natural killer cells, natural killer T cells and DCs expressed mRNA for the IL-7 receptor α-chain (**Fig. 3a**). FRCs expressed the B cell–survival factor and T cell–costimulator BAFF[17]. FRCs also produced transcripts encoding molecules that support myeloid cells, including IL-34, which binds the receptor for macrophage colony-stimulating factor 1 (ref. 18); the cytokine Flt3L, shown to bind the receptor tyrosine kinase Flt3 and to support the development, maintenance and population expansion of DCs[19]; and the monocyte-DC

chemoattractant CXCL14 (**Fig. 3a,b**). DNCs also expressed many of these factors, albeit in much lower amounts.

FRCs also regulate lymph node vasculature[20]. They expressed VEGF-A, as reported[20], and we detected transcripts for several other angiogenic regulatory molecules, including VEGF-C, ANGPTL2, HGF, GREM1 and SERPINF1 (**Fig. 3a**). DNCs shared the expression of some of those factors, whereas ECs expressed the relevant receptors (**Fig. 3a**). ECs produced fibroblastic growth factors, including PDGFA, PDGFB, PDGFC and PDGFD, which suggested a dynamic codependence between FRCs and ECs.

FRCs dominated chemokine production, although here too DNCs resembled FRCs (**Fig. 3b**). As expected, FRCs produced large amounts of transcripts for the chemokines CCL19 and CCL21a, whereas relevant hematopoietic subsets expressed the chemokine receptor CCR7 (**Fig. 3b**). Although we detected little CCL19 mRNA in ECs, in agreement with published reports[2], BECs showed substantial expression of

Figure 2 Unbiased analysis of LNSCs provides insight into FRC function. (**a**) Comparison of the expression profiles of FRCs with those of BECs (top) or LECs (bottom), for SLNs and MLNs; probes along diagonals have similar expression in both sites. Colors indicate probes upregulated in SLN FRCs (blue) or in SLN BECs (gray, top) or SLN LECs (gray, bottom; FC > 2, EV > 120 for at least one LNSC subset, and CV < 0.5 for all LNSCs). Numbers in quadrants indicate number of probes in each. vs, versus. (**b**) Projection of probes identified in **a** onto volcano plots of SLN FRCs and SLN LECs (top) or SLN BECs (bottom). Numbers in quadrants indicate total number of probes of that color on that side of the vertical axis. $P < 0.0001$ (χ^2 test). (**c**) Comparison of BEC and LEC expression profiles; colors indicate probes upregulated in BECs (blue) or LECs (gray; values as in **a**). (**d**) Enrichment in KEGG pathways for probes upregulated in FRCs relative to their expression in ECs or vice versa ($\delta = 1.0$ (adjusted FC ≥ 2)

for at least one comparison, and $\delta = 0.85$ (adjusted FC ≥ 1.8) for all other comparisons; $P < 0.05$ for differences in expression). Blue indicates KEGG pathways with the most significant enrichment (Benjamini procedure; KEGG accession code in parentheses): focal adhesion (mmu04510), ECM-receptor interactions (mmu04512), cytokine–cytokine receptor interactions (mmu04060), cancer pathways (mmu05200), glutathione metabolism (mmu00480), cell-adhesion molecules (mmu04514), adherens junction (mmu04520), VEGF signaling pathway (mmu04370), axon guidance (mmu04360) and leukocyte transendothelial migration (TEM; mmu04670). Data are representative of one experiment with four to five independent replicates.

CCL21a (**Fig. 3b**). Unexpectedly, in FRCs we found considerable transcription of CXCL13, a B cell chemoattractant reportedly restricted to follicular dendritic cells and a minor MAdCAM-1^{+} population of marginal reticular cells. We did not detect follicular dendritic cells in our cell preparations, on the basis of expression of their canonical markers CD21, CD35 and FcεRII (**Supplementary Fig. 3a,b**). We determined whether marginal reticular cells were responsible for the observed CXCL13 expression by sorting MAdCAM-1^{−} FRCs and MAdCAM-1^{+}gp38^{+}CD140a^{+}CD31^{−} marginal reticular cells. Both subsets had similar expression of CXCL13, as assessed by PCR (**Supplementary Fig. 3c**). Consistent with the PCR data, MAdCAM1^{−} and bulk SLN FRCs had a similar abundance of CXCL13 transcripts, as measured by microarray (**Supplementary Fig. 3d**).
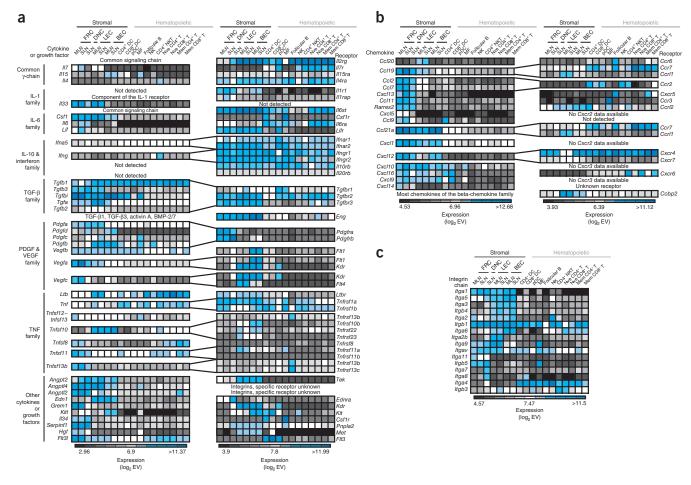
FRCs transcribed other chemokines, such as CCL2 and CCL7, that may facilitate the recruitment or organization of receptor-expressing memory T cells and DCs (**Fig. 3b**). FRCs were the main source of the lymphocyte chemoattractant CXCL12, with more than twice as much expression as that in BECs and DNCs. LECs uniquely expressed CCL20 (**Fig. 3b**), which is suggested to promote the egress of activated T cells from lymph nodes[21]. Memory T cells and B cells had the highest expression of CCR6 transcripts, which suggested that CCL20 may be relevant to these populations. Together these data indicated that LNSCs were important in regulating hematopoietic-cell recruitment to and localization within secondary lymphoid organs.

Integrins help shape cell-cell and cell-ECM interactions; we therefore examined LNSC integrin-expression profiles. Although subsets shared expression of certain integrin chains, such as integrins α_1, α_5 and β_1, the expression of other chains had a more restricted pattern (**Fig. 3c**). In fact, DNCs expressed little integrin α_2, in contrast to FRCs, LECs and BECs, and this was also evident at the protein level (**Fig. 3c** and **Supplementary Fig. 2c,d**). Meanwhile, FRCs and DNCs shared expression of the integrin chains α_{11} and β_5, whereas among LNSCs, DNCs uniquely expressed the integrin chains α_7, α_8 and α_4. These data suggested that stromal subsets support hematopoietic cells as well as each other via complex regulatory networks.

Identification of previously unknown conduit-network components

FRCs create unique yet poorly studied conduits that deliver small, lymph-borne factors to the cortex faster than filtration through cell-dense tissue would allow. At the conduit center lies a collagen-rich core, enveloped by a microfibrillar zone that contains fibrillins and the antigen recognized by the monoclonal antibody ER-TR7 (ref. 9; **Supplementary Fig. 4a**). Surrounding the microfibrillar zone is a basement membrane ensheathed by FRCs[9]. As FRCs showed enrichment for higher expression of genes encoding molecules involved in ECM-receptor interactions (**Fig. 2d**), we examined the transcription and secretion of conduit components by FRCs (**Fig. 4**).

In addition to expressing collagens I and IV[9], FRCs expressed transcripts for collagens III, V, VI, XIV and XVI (**Fig. 4a**). DNCs resembled FRCs in their expression of these molecules. BECs had the highest expression of collagen XV, whereas LECs and DNCs shared expression of collagen XII. Immunofluorescence microscopy showed ensheathment of collagen XIV by ER-TR7, which placed it in the collagen core (**Fig. 4c** and **Supplementary Figs. 4b** and **5**). Collagen VI, however, mostly localized together with ER-TR7, which localized it to the microfibrillar zone (**Fig. 4d** and **Supplementary Figs. 4f** and **6**).

FRCs can regulate conduit structure and organization through the secretion of molecules such as small leucine-rich proteoglycans (SLRPs). SLRPs regulate collagen fibrillogenesis, bridge collagen I fibrils to the basement membrane and interact with growth factors[22]. FRCs had high expression of the SLRPs lumican, fibromodulin, osteoglycin, decorin, biglycan and prolargin (**Fig. 4a**). As detected by immunofluorescence microscopy, decorin, biglycan and fibromodulin were surrounded by ER-TR7 and localized to the conduit core (**Fig. 4c** and **Supplementary Figs. 4c–e**, **7** and **8**).

The conduit basement membrane contains laminin-8 ($\alpha4\beta1\gamma1$) and laminin-10 ($\alpha5\beta1\gamma1$)[9], which were expressed by all LNSCs (**Fig. 4a**). FRCs expressed the laminin chains $\alpha2$, $\alpha3$ and $\gamma3$ (**Fig. 4a**), which suggested that other laminins may also contribute to conduit structure and function. FRCs expressed transcripts for the glycoprotein vitronectin, which promotes cell adhesion and spreading, inhibits the membrane-attack complex of the complement system and prevents

Figure 3 Expression of cytokines, growth factors and immunologically relevant receptors by stromal and hematopoietic cell subsets. (**a**) Heat-map analysis of the expression of cytokines, growth factors and receptors by LNSCs and 11 lymph node hematopoietic subsets (EV > 120 for the receptor or ligand in any stromal population), for log₂-transformed data. pDC, plasmacytoid DC; MF, macrophage; B, B cell; NK, natural killer cell; NKT, natural killer T cell; Nve, naive; T, T cell; Mem, memory. (**b**) Analysis of the expression of chemokines and chemokine receptors as in **a**. (**c**) Analysis of the expression of integrins as in **a**. Data are representative of one experiment with three to five independent replicates (mean values).
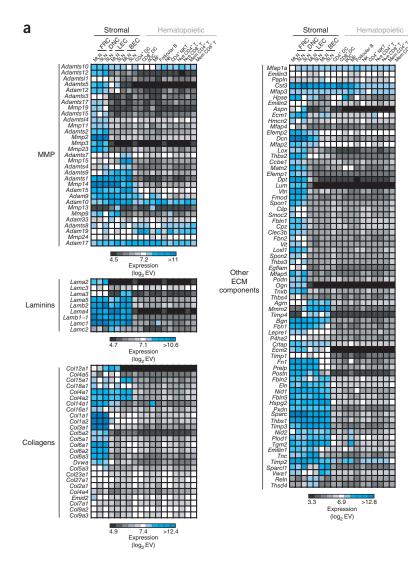
interactions between plasminogen activator inhibitor-1 and the ECM[23]. Vitronectin has been detected mainly in B cell follicles, but it also shows a reticular pattern in the T cell zone[24]. We found that vitronectin decorated the surface of ER-TR7+ fibers, forming cage-like structures at conduit branch points (**Fig. 4e** and **Supplementary Figs. 4g** and **9**) and was wrapped by α-SMA+ FRCs, which localized it to the basement membrane (**Supplementary Fig. 4h**).

Lymph nodes undergo considerable expansion and contraction during immune responses, often within a matter of hours, which suggests extensive remodeling of the ECM to accommodate these changes. Matrix metalloproteinases (MMPs), which are important for turnover of the ECM in extranodal tissues as well[25], were expressed by LNSCs (**Fig. 4a**). The abundance of transcripts for MMP2 and MMP3 was greatest in FRCs and DNCs, whereas FRCs, DNCs and LECs had substantial expression of transcripts for MMP9 and MMP14 (**Fig. 4a**). In contrast, BECs had the highest expression of MMP15. LECs and BECs also had higher expression of mRNA and protein of the metallopeptidase ADAM10 than did FRCs or DNCs (**Fig. 4a,b**). FRCs produced large amounts of transcripts for molecules involved in matrix and elastic fiber assembly, including LOX, LOXL1, MFAP-2, MFAP-5 and FBLN1 (**Fig. 4a**). These data described a more complex picture of conduit structure and ECM maintenance by FRCs than previously realized.

Organ-specific specialization of fibroblastic stroma

FRCs are thought to be highly specialized to the lymphoid microenvironment, but in-depth comparisons with other fibroblast populations have not been made. We analyzed CD45−gp38+CD31−CD140a+ skin fibroblasts (SFs), sorted to high purity (n = five mice per replicate; **Supplementary Fig. 10a–c**), and MTS-15+ thymic fibroblasts (ThFs). We computed population distances for probes with different expression through the use of PCA, correlation scores and Euclidean distances (**Fig. 5a–c**). Lymph node FRCs were most similar across all metrics. PCA and Euclidean distance suggested that FRCs were more like SFs, whereas correlation scores indicated higher concordance between SFs and ThFs.

We mapped the genes that distinguished SLN FRCs, ThFs and SFs by pairwise comparisons (δ = 1.0 (adjusted FC ≥ 2); P < 0.05 for differences in EV; **Supplementary Table 3**) to KEGG pathways. Presentation of the enriched pathways (P < 0.05, Benjamini procedure) on P value–by–P value plots identified five biologically interesting results (**Fig. 5d**). FRC-specific probes showed unique enrichment for the cytokine–cytokine receptor pathway, as shown by this pathway's position on the FRC plot (**Fig. 5d**). Notably, relative to SF-specific probes, FRC-specific and ThF-specific probes were biased toward genes encoding molecules involved in antigen presentation and cell contraction (**Fig. 5d**). SFs showed enrichment for higher expression
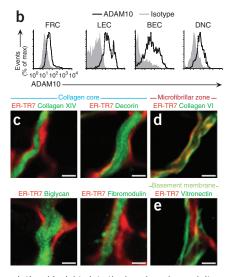
Figure 4 Transcriptional insights into the lymph-node conduit network. (**a**) Identification of proteinaceous ECM components by gene ontology (AmiGO database), presented as heat maps of expressed probes (EV > 120 for any LNSC population) for log_2-transformed data; blue indicates higher expression. (**b**) Expression of ADAM10 (black lines) by freshly isolated SLN FRCs, LECs, BECs and DNCs, assessed by flow cytometry. Isotype (gray shading), isotype-matched control antibody. (**c**) Confocal immunofluorescence microscopy of reticular fibers in the T cell zone stained for the ER-TR7 antigen (red) and the following collagen core components (green): collagen XIV (top left), decorin (top right), biglycan (bottom left) and fibromodulin (bottom right). (**d**) Confocal microscopy as in **c**, with staining for the ER-TR7 antigen (red) and the microfibrillar zone constituent collagen VI (green). (**e**) Confocal microscopy as in **c**, with staining for the ER-TR7 antigen (red) and vitronectin (green), newly identified as being localized to the basement membrane. Scale bars (**c–e**), 2 μm. Data are representative of one experiment with three to five independent replicates (**a**), three independent experiments with seven mice (**b**) or four to five independent experiments (**c–e**).

of genes encoding molecules that serve classical fibroblast functions involving ECM-receptor interactions (**Fig. 5d**).

FRCs had higher expression than SFs had of many components of the major histocompatibility complex (MHC) class I pathway, including antigen-processing machinery and canonical and noncanonical MHC class I molecules (**Supplementary Fig. 10d**). ThFs, SLN ECs and hematopoietic cells also had a greater abundance of such transcripts, which suggested that lymphoid-tissue environments might enhance transcription of these genes. Although FRCs had higher expression of some components of the MHC class II pathway than did SFs, this expression was much lower than that in 'professional' antigen-presenting cells (**Supplementary Fig. 10d**).

In addition to presenting self antigens, FRCs regulate the recruitment of cells of the immune response to lymph nodes and their homeostasis within lymph nodes. Although FRCs, SFs and ThFs produced transcripts for similar chemokines and cytokines, the transcript abundance was much greater in FRCs (**Supplementary Fig. 10d**). This reflected the functional specialization of these lymph-node residents.
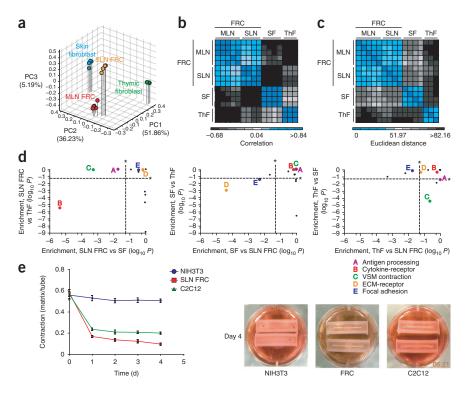
KEGG analysis suggested that FRCs and ThFs were more biased toward contractile ability than were SFs (**Fig. 5d**). FRCs express α-SMA, and their contractility has been demonstrated by a wrinkle assay[2]. Although FRCs had much higher expression of α-SMA and smooth muscle myosin light chain than did SFs or ThFs (**Supplementary**

Fig. 10d), both FRCs and ThFs produced a greater abundance of transcripts for other smooth muscle-associated genes (**Supplementary Fig. 10d**). Consistent with their expression profile, FRCs had stronger contractile function than did NIH3T3 mouse fibroblasts, on par with that of C2C12 mouse myoblasts (**Fig. 5e**).

The production and maintenance of ECM are fundamental characteristics of fibroblasts. KEGG pathway analysis suggested that SFs were most specialized in these functions (**Fig. 5d**). Notably, whereas all fibroblastic populations shared expression of most ECM components, FRCs uniquely expressed certain ECM or matrix-regulatory molecules or shared expression of those molecules with ThFs (**Supplementary Fig. 10d**). In contrast to SFs, FRCs and ThFs had considerable transcription of MMP9. FRCs also had the highest expression of the ECM-remodeling molecules MMP23 and heparanase and the conduit components vitronectin and fibromodulin (**Supplementary Fig. 10d**). Together these data demonstrated that FRCs shared an unexpectedly large number of characteristics with their skin and thymic counterparts, but they were nonetheless specialized to their unique microenvironment.

Cadherin-11 identifies cell-cell junctions between FRCs

FRCs interacted closely with each other as they ensheathed the reticular fibers that they secreted (**Supplementary Fig. 11**); however,

Figure 5 Transcriptional specialization of FRCs, ThFs and SFs. (**a**) PCA of the 15% of probes with the greatest difference in expression among SLN FRCs, MLN FRCs, SFs and ThFs, for $\log_2$-transformed and row- and column-standardized EVs. (**b**) Heat map of correlation values (Pearson coefficient) for the 15% of probes with the greatest difference in expression identified in **a**, calculated with $\log_2$-transformed and row-standardized data. Blue indicates highest correlation. (**c**) Heat map of Euclidean distances for the 15% of probes with the greatest difference in expression identified in **a** (data transformed as in **b**). Blue indicates samples with the smallest distance. (**d**) Scatter plots of significant results from pooled KEGG pathway-enrichment analyses of cell type–specific lists generated from pairwise delta-score and multiplot analyses ($\delta = 1$ (adjusted FC ≥ 2), $P < 0.05$). P values (Benjamini procedure) are presented in terms of pathway enrichment in FRCs (left), SFs (middle) or ThFs (right). Colored letters indicate biologically notable results (KEGG accession code in parentheses): A, antigen processing and presentation (mmu04612); B, cytokine–cytokine receptor interactions (mmu04060); C, vascular smooth muscle contraction (mmu04270); D, ECM-receptor interactions (mmu04512); E, focal adhesion (mmu04510). (**e**) Comparison of the contractile activity of FRCs, NIH3T3 fibroblasts and C2C12 myoblasts *in vitro*. *$P < 0.05$ (Benjamini procedure). Data are representative of one experiment with three to five independent replicates (**a**–**d**) or two experiments (**e**; mean ± s.d.).

little is known about these junctions. We examined the expression of candidate cell-adhesion molecules by LNSCs and observed high expression of cadherin-11 by FRCs (**Fig. 6a**). Cadherin-11 is a member of the calcium-dependent cadherin family of adhesion molecules[26]. Expression of cadherin-11 in the lymph node has been observed before[27]; however, its specific localization has remained unknown. Notably, we also observed transcripts for cadherin-11 in SFs and ThFs (and, to a lesser extent, DNCs; **Fig. 6a**), which reflected a common mesenchymal origin of these cells[26]. We confirmed, by flow cytometry, surface expression of cadherin-11 on freshly isolated FRCs (**Fig. 6b**). In accordance with the microarray data, ECs had little to no expression of cadherin-11, DNCs had some expression and hematopoietic cells were distinctly negative for this molecule (**Fig. 6b**).

Cadherin molecules form homotypic interactions, binding cadherins of the same type in adjacent cells and interacting laterally within a single cell[26]. We evaluated the localization of cadherin-11 on populations of FRCs expanded *in vitro* and found they maintained surface expression of this protein (**Fig. 6c**). We observed cadherin-11, by immunofluorescence microscopy, in junctions between adjacent FRCs (**Fig. 6d**), as shown in fibroblast-like synoviocytes[26]. The specific expression of cadherin-11 in FRCs suggested that it may contribute to FRC-FRC interactions.

DNCs are contractile pericytes

Several groups have reported the existence of DNCs[2,6,7], which constitute 5–10% of LNSCs yet have unknown lineage, localization, phenotype and function. It is unclear whether DNCs encompass highly tolerogenic extrathymic cells that express the transcriptional regulator Aire[5]. Unlike those extrathymic Aire-expressing cells, DNCs do not express the adhesion molecule EpCAM[6] but are the only LNSC subset known to transcribe even small amounts of Aire[6,7], although Aire protein has not been noted[6]. Among LNSCs, DNCs uniquely

lack expression of Toll-like receptor 3 (TLR3)[6] and have different expression of peripheral tissue–restricted antigens[6]. DNCs lack many surface proteins characteristic of other LNSCs. As part of our sorting strategy, we chose to further define DNCs as CD44−, as we found that this combination excluded contaminating CD45loCD44+ cells.

Throughout our analysis, DNCs resembled FRCs. We compared DNCs with other LNSCs by two-class EV-versus-FC plots. DNCs and FRCs differed in the expression of 834 probes (FC ≥ 2; **Fig. 7a**). In contrast, DNCs and ECs varied in expression of more than 1,880 probes (**Fig. 7b,c**). Thus, the transcriptional profiles of DNCs and FRCs were similar despite considerable differences in surface phenotype[6]. We identified probes specific to SLN DNCs and FRCs ($\delta = 1.0$ (adjusted FC ≥ 2); $P < 0.05$ for differences in EV in DNCs versus FRCs; **Supplementary Table 4**). MLN DNCs closely resembled SLN DNCs in the expression of genes measured by these probes (data not shown). By DAVID analysis, the list of FRC-specific probes showed enrichment for genes encoding molecules involved in cytokine-cytokine receptor interactions. In contrast, DNCs had high expression of genes encoding molecules with structural and contractile functions and had KEGG profiles reminiscent of those of cardiomyocytes and smooth-muscle cells (**Fig. 7d**). We assessed genes encoding molecules important for smooth-muscle contraction, including actin subtypes and myosin chains (**Fig. 7e**). Of those genes, the expression of *Actg2* and *Myh11* is described as being specific to smooth muscle cells[28], whereas the expression of others is common to multiple cell types. Notably, whereas α-SMA is often used as a surrogate marker for FRCs, DNCs had the highest expression of transcripts for this protein (**Fig. 7e**).

We next sought potential markers to delineate the conceivably heterogenous 'bulk-negative' (gp38−CD31−CD45−CD44−) DNC population, hoping to assign it a lymph-node microniche and probable function. The following two candidates arose: calponin-1

Figure 6 Cadherin-11 identifies junctions between lymph-node fibroblastic reticular cells. (**a**) Expression of candidate cell-adhesion molecules in stromal and hematopoietic cells, for log$_2$-transformed data. (**b**) Expression of cadherin-11 (black lines) in freshly isolated FRCs, LECs, BECs, DNCs and bulk hematopoietic cells, assessed by flow cytometry. (**c**) Surface expression of cadherin-11 on a population of FRCs expanded *in vitro*, assessed by flow cytometry. (**d**) Confocal immunofluorescence microscopy of cadherin-11 (green) on a population of FRCs expanded *in vitro* (red, F-actin; blue, DAPI (DNA-intercalating dye)). Scale bar, 10 μm. Data are representative of one experiment with three to five independent replicates (**a**) or four independent experiments (**b**–**d**).
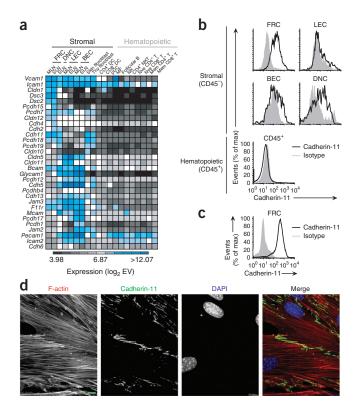

(CNN1) and integrin α$_7$ (ITGA7; **Fig. 7f**). CNN1 is an actin-associated protein specific to smooth muscle cells and is a chief regulator of force production in contractile cells[28]. ITGA7 pairs with integrin chain β$_1$ to bind laminin-1, laminin-2 and laminin-4 in the basement membrane and is important for linking muscle fibers to the ECM[29]. Indeed, we found that sorted DNCs grew in culture only when supplemented with Matrigel (a gel consisting of basement-membrane proteins) and formed strong contractile attachments to the matrix (**Fig. 7g**).

Analysis with antibody to CNN1 (anti-CNN1) and anti-ITGA7 identified DNCs as pericyte-like cells, surrounding some medullary and cortical vessels (**Fig. 7h,i**). There were no apparent morphological differences between vessels with or without these cells. Staining with anti-CNN1 also identified an elongated, subcapsular DNC subset limited to the medullary face of the lymph node. This subset was not stained by anti-ITGA7 (data not shown). By flow cytometry, however, it was apparent that staining with anti-CNN1 identified a small minority (<5%) of DNCs, whereas anti-ITGA7 stained >50% of DNCs (**Supplementary Fig. 12**), which suggested that pericytes were the main population of DNCs. These data identified most DNCs as fibroblastic, contractile pericytes, which we called 'ITGA7$^+$ pericytes' (IAPs).

Inflammation triggers transcriptional changes in LNSCs

FRCs, LECs, BECs and IAPs are positioned at key sites throughout the lymph node to encounter lymph-borne molecules, and their steady-state transcriptional profiles suggested they are poised to respond to inflammatory or infectious insults. To investigate the responses of stromal cells to inflammation and ongoing immune responses, we transferred 1.5 × 10^6 OT-I T cells (which have transgenic expression of an ovalbumin-specific T cell antigen receptor) intravenously into 5-week-old C57BL/6 mice. At 18 h after T cell transfer, we gave mice intravenous injection of 30 μg lipopolysaccharide from *Escherichia coli* (serotype O127:B8) and 500 μg ovalbumin (**Supplementary Fig. 13a**). We isolated FRCs, LECs and BECs from SLNs (*n* = 5–6 mice per replicate) 12 h after injection of mice with lipopolysaccharide and ovalbumin and sorted the cells to high purity (called '12 h cells' or '12 h mice' here; **Supplementary Fig. 13b**). Because of the rarity of IAPs, we did not sort this subset for further analysis.
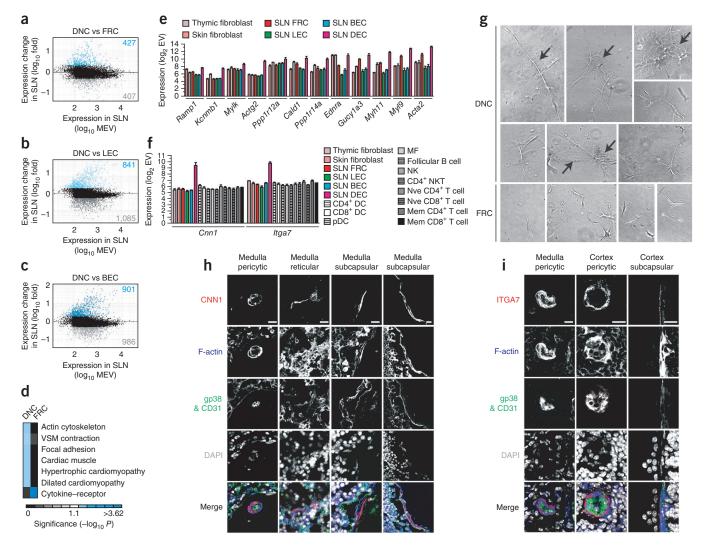
Treatment changed the transcriptional profiles of FRCs, LECs and BECs considerably, as demonstrated by hierarchical clustering of 373 probes with different expression (FC > 2, *P* < 0.05) in 12 h stromal subsets and in their corresponding untreated counterparts (**Fig. 8a**). We identified 113 such probes for further study (δ = 1.0 (adjusted FC ≥ 2); *P* < 0.05 for differences in EV for SLN FRCs from 12 h mice versus SLN FRCs from untreated mice, and so on; **Supplementary Table 5**). Probes upregulated in 12 h FRCs and BECs showed substantial enrichment for the KEGG antigen-processing and

antigen-presentation pathway, in contrast to probes upregulated in 12 h LECs (**Fig. 8b**). Probes downregulated after treatment of mice did not show enrichment for particular KEGG pathways.

Projection of the 113 probes onto FC–versus–*P* value plots of stromal subsets isolated from 12 h mice and untreated mice resulted in similar probe distributions, although FRCs seemed to respond most strongly at this time point, as FCs were generally largest for this subset (**Fig. 8c**). Consistent with their residence in an inflammatory milieu, 12 h FRCs demonstrated enhanced expression of genes encoding molecules involved in the acute-phase response (including SAA3, A2M, and SERPINA1B), whereas all three subsets has more mRNA encoding the inflammatory chemokines CCL5 and CXCL9 (**Fig. 8c**). In addition, transcripts of many genes that are inducible by interferons or TLR4 signaling or genes encoding molecules that regulate these pathways, such as IRF7 (ref. 30), LY6A[31] and LCN2 (ref. 32), were upregulated in 12 h stroma (**Fig. 8c**). The 12 h stromal subsets had less mRNA for NR1D1, a negative regulator of TLR4 signaling[33]. We observed that although they were not part of the 113-probe list, transcripts for IL-7 and IL-33 were also significantly upregulated in 12 h FRCs (2.6-fold, *P* = 0.003 (IL-7); 1.9-fold, *P* = 0.001 (IL-33)). The expression of transcripts for a variety of ECM-associated molecules (such as MMP9, POSTN, COL6A6, and LAMA2) was significantly downregulated in FRCs after treatment of mice with lipopolysaccharide and ovalbumin, and we also observed this trend to a lesser degree in LECs and BECs (**Fig. 8c**).
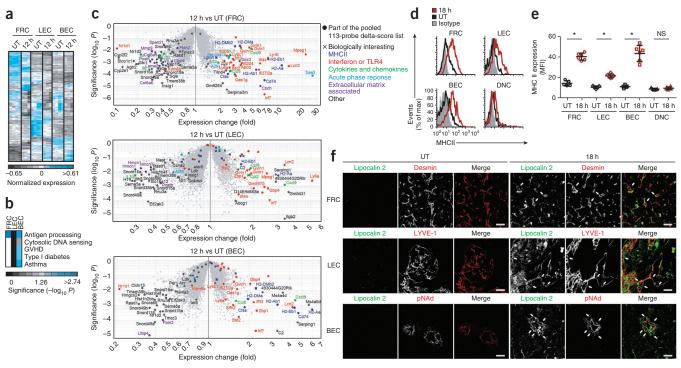
In accordance with the results obtained by KEGG pathway analysis, we found that 12 h FRCs and BECs had upregulated expression of many components of the MHC class II presentation pathway, including chains of MHC class II molecules (H2-Aα, H2-Aβ1 and H2-Eβ1), the invariant chain (CD74), CTSS, H2-DMα and H2-DMβ2 (**Fig. 8c**). Furthermore, 12 h FRCs also had significantly higher expression of LGMN (**Fig. 8c**). By flow cytometry,

Figure 7 DNCs are contractile pericytes. (**a**) Comparison of gene expression by SLN DNCs and FRCs (two-class EV-versus-FC plots). Colors indicate probes upregulated in DNCs (blue) or FRCs (gray; EV > 120 for any LNSC subset, FC > 2, CV < 0.5). Numbers in corners indicate total upregulated probes. MEV, two-class mean EV. (**b,c**) Analysis of SLN DNCs and LECs (**b**) or BECs (**c**) as in **a**. (**d**) Enrichment in KEGG pathways for probes upregulated in SLN DNCs relative to SLN FRCs or vice versa (δ = 1 (adjusted FC ≥ 2), *P* < 0.05). Blue indicates KEGG pathways with the most significant enrichment (Benjamini procedure; KEGG accession code in parentheses): regulation of actin cytoskeleton (mmu04810), vascular smooth muscle contraction (mmu04270), focal adhesion (mmu04510), cardiac muscle contraction (mmu04260), hypertrophic cardiomyopathy (mmu05410), dilated cardiomyopathy (mmu05414) and cytokine–cytokine receptor interactions (mmu04060). (**e**) Expression by LNSCs, SFs and ThFs of 12 vascular smooth muscle–associated genes upregulated in DNCs relative to FRCs. (**f**) Stromal and hematopoietic expression of the candidate DNC markers CNN1 (*Cnn1*) and ITGA7 (*Itga7*). (**g**) Brightfield microscopy of sorted FRCs and DNCs grown for 5 d in a three-dimensional Matrigel. Arrows indicate visible matrix contraction. Original magnification, ×100. (**h**) Immunofluorescence microscopy of ITGA7, F-actin and DAPI; exclusion of staining for gp38 and CD31 indicates cells are DNCs. Scale bars, 15 μm. (**i**) Immunofluorescence microscopy of CNN1, F-actin and DAPI as in **h**. Scale bars, 15 μm. Data are representative of one experiment with three to four independent replicates (**a–f**; mean and s.d. in **e,f**) or three independent experiments (**g–i**).

we investigated the surface expression of MHC class II on SLN FRCs, LECs, BECs and DNCs isolated from mice 18 h after injection of lipopolysaccharide and ovalbumin (**Fig. 8d,e**). After treatment, surface expression of MHC II was significantly higher on FRCs, LECs and BECs but not on DNCs. Consistent with the microarray data, FRCs and BECs demonstrated larger increases in MHC class II expression than did LECs (**Fig. 8d,e**).

LCN2 is a multifaceted, lipopolysaccharide-inducible molecule that has been linked to host defense against *Escherichia coli*, *Klebsiella pneumoniae* and *Mycobacterium tuberculosis*[32]. Given the substantially higher expression of LCN2 by FRCs, LECs and BECs after treatment (17.5-fold, 3.5-fold and 4.8-fold higher, respectively),

we obtained SLNs from untreated mice and from mice 18 h after injection of lipopolysaccharide and ovalbumin and stained sections from these tissues with anti-LCN2, anti-desmin (to identify FRCs), anti-LYVE-1 (to identify LECs) and anti-pNAd (to identify BECs; **Fig. 8f**). In contrast to FRCs, LECs and BECs in SLN sections from untreated mice, all three stromal subsets had detectable expression of LCN2 18 h after treatment (**Fig. 8f**). In agreement with published reports[32], we detected LCN2 in desmin-negative, LYVE-1⁻ and pNAd⁻ cells; these were probably of hematopoietic origin (data not shown). These data reinforced the idea that LNSCs are poised to respond to inflammatory or infectious triggers and may contribute as active participants during ongoing immune responses.

Figure 8 LNSC response to inflammation. (**a**) Unbiased hierarchical clustering of 373 probes with different expression in the corresponding stromal subsets from untreated (UT) or 12 h mice (EV > 120 for either population, FC > 2 and CV < 0.5 within each population), for $\log_2$-transformed, row-mean-centered and row-normalized data. (**b**) Enrichment in KEGG pathways for probes upregulated in 12 h LNSCs ($\delta = 1.0$ (adjusted FC $\geq$ 2); $P < 0.05$). Blue indicates KEGG pathways with the most significant enrichment (Benjamini procedure; KEGG accession code in parentheses): antigen processing and presentation (mmu04612), cytosolic DNA-sensing pathway (mmu04623), graft-versus-host disease (mmu05332), type I diabetes mellitus (mmu04940) and asthma (mmu05310). (**c**) Projection of the 113 probes identified in **b** onto volcano plots of FRCs, LECs and BECs from untreated or 12 h mice. Key indicates biological categorization of probes. MHCII, MHC class II. (**d**) Surface expression of MHC class II on SLN LNSCs from untreated mice and mice treated for 18 h, assessed by flow cytometry. (**e**) Median fluorescence intensity (MFI) of the expression in **d**. Each symbol represents an individual mouse; horizontal lines indicate mean (± s.d.). (**f**) Confocal immunofluorescence microscopy of sections of SLNs from untreated mice and mice treated for 18 h, stained for LCN2 (green) and desmin (red; FRCs), LYVE-1 (red; LECs) or pNAd (red; BECs). Arrows indicate LCN2⁺ stroma. Scale bars, 25 μm. Data are representative of one experiment with three to four independent replicates (**a**–**c**) or two independent experiments with five to six mice per condition (**d**–**f**).

DISCUSSION

The lymph-node conduit network is a complex molecular sieve that rapidly delivers low-molecular-weight lymph-borne molecules deep into the cortex[9]. This unique ability to exclude molecules by size is key to conduit function, yet its molecular basis is poorly understood. Our delineation here of the expression of ECM components by FRCs has identified a potential mechanism for regulating conduit structure and function.

We found that in addition to containing collagen I, which assembles into long fibrillar chains, providing tensile strength, the collagen core contained collagen XIV, which crosslinks collagen I, limiting fibril diameter by preventing lateral binding of adjacent fibrils[34]. The SLRP decorin, which also has high expression in the conduit core, is another key regulator of fibril diameter[35]. Finally, LOX covalently crosslinks collagen I–collagen XIV bonds, locking the low-diameter arrangement[36]. Macromolecular diffusion studies have reported that collagen fibrils have pore-like permeability dependent on tertiary and quaternary structure[37]. Tight regulation of fibril diameter and packing conceivably control pore size; dysregulation could impair the delivery of small molecules to the lymph-node parenchyma and alter the structural integrity of the network. We suggest that the exclusion of molecules by size in conduits is a property of the type I collagen core tightly regulated by collagen XIV and SLRPs. Future studies should define the roles of these factors in regulating fibril density and diameter in lymph nodes.

The transcriptional profiles of LNSCs suggested that these cells may be poised to respond via lymph-borne infectious or inflammatory cues.

Although LNSCs lacked transcripts for NALP3, part of the inflammasome that recognizes influenza and adenovirus[38], FRCs and DNCs produced more transcripts for the interferon-inducible transmembrane protein IFITM-1 than did other populations profiled. Furthermore, LNSCs had higher expression of IFITM-2 and IFITM-3 than did hematopoietic cells. IFITM-1, IFITM-2 and IFITM-3 have been linked to host defense against influenza virus, West Nile virus and Dengue virus[39]. Ligation of TLR3, another virus-recognition receptor, results in less activation of T cells by FRCs[6]. Exposure of LNSCs to infectious agents is hypothesized to preserve lymph-node architecture by promoting stromal resistance to destruction mediated by the immune system[6,40].

We found that FRCs, LECs and BECs, all of which express TLR4 in the steady state, responded vigorously to the onset of inflammation by upregulating expression of interferon-and/or TLR4-inducible genes, as well as genes encoding molecules that regulate these pathways, molecules involved in the acute-phase response, the inflammatory chemokines CCL5 and CXCL9, and key components of the MHC class II antigen-processing and antigen-presentation pathway. Notably, expression of various chains of MHC class II molecules (H2-Aα, H2-Aβ1 and H2-Eβ1), the invariant chain (CD74), CTSS, H2-DMα and H2-DMβ2 was higher in FRCs and BECs after the onset of inflammation. FRCs also upregulated LGMN. Surface expression of MHC II was indeed higher on FRCs, LECs and BECs 18 h after injection of lipopolysaccharide and ovalbumin, whereas its expression remained unchanged on DNCs. The presentation of antigens by LNSCs via

MHC class II may contribute to the induction of CD4^{+} T cell tolerance or the generation of regulatory T cells in inflammatory settings or during chronic immune responses. Future studies should elucidate the role of the MHC class II antigen-processing and antigen-presentation pathway in LNSCs under inflammatory conditions. We also found that FRCs, LECs and BECs produced LCN2, a potent antimicrobial iron-sequestering molecule[32], after the onset of inflammation. The secretion of LCN2 by LNSCs may limit bacterial expansion during early stages of infection by decreasing the availability of iron[32].

Although FRCs are residents of secondary lymphoid organs, similarly specialized fibroblasts appear at sites of chronic inflammation (tertiary lymphoid organs) and in tumors, where they support lymph node–like environments[13,14]. These FRC-like cells are often associated with poor clinical outcomes[13,14]. Controlling the development of tertiary lymphoid organs is therefore an important therapeutic aim; however, fibroblastic populations from various tissues have not been systematically compared. We examined the transcriptomes of FRCs, ThFs and SFs to study the specialization of fibroblasts in lymphoid organs. Despite sharing many characteristics, each population had a distinctive profile. Both FRCs and ThFs were better equipped than SFs for antigen presentation and contractility. Exposure to immune mediators and lymph flow[41] probably regulates the FRC transcriptome. FRCs uniquely showed enrichment for higher expression of genes encoding molecules involved in cytokine–cytokine receptor interactions, which further demonstrated immune-related specialization.

In contrast to interstitial fibroblasts, FRCs interact closely with each other along the conduits that they ensheath[42]; however, little is known about these cell-cell contacts. We found that cadherin-11 localized to junctions between FRCs. We also observed transcripts for cadherin-11 in ThFs and SFs, which reflected a common mesenchymal origin. Upregulation of cadherin-11 is associated with more division, adhesion, bone infiltration and production of inflammatory cytokines and altered production of ECM by fibroblast-like synoviocytes in rheumatoid arthritis[26,43]. Future studies should determine whether cadherin-11 signaling in FRCs regulates similar processes.

LNSCs interact closely with hematopoietic cells. Accordingly, we examined lymph-node stromal and hematopoietic niches for previously undescribed aspects of crosstalk. A notable finding was shared stromal expression of many genes thought to be subset restricted. FRCs and, to a lesser extent, DNCs produced transcripts for cytokines and chemokines that may act on memory T cells, DCs, B cells, macrophages and natural killer cells, which probably contributes to their recruitment, organization and survival. FRCs had the highest expression of transcripts for Flt3L among the stromal and hematopoietic subsets profiled, which suggested a previously unknown role for FRCs in maintaining lymph node–resident DCs, similar to thymic stroma[44]. Meanwhile, CCL20 expression by LECs may contribute to the steady-state egress of memory T cells or B cells. Although FRCs produced substantial quantities of transcripts for CCL19 and CCL21a, as reported before[2], we observed lower expression in other LNSCs. In addition, both FRCs and LECs transcribed the gene encoding IL-7, in contrast to published reports[2]. Furthermore, FRCs, BECs and DNCs had high expression of the homeostatic chemokine CXCL12. Unexpectedly, we observed CXCL13 expression in FRCs. Microscopy confirmed localization of CXCL13 to B cell follicles, where rare FRCs ensheath sparse conduits[45]. We found that 11.6% ± 8.2% of areas with bright CXCL13 were associated with desmin-positive FRCs surrounding ER-TR7^{+} conduits (data not shown), which suggested that FRCs in the B cell zone may form a discrete CXCL13-expressing subset. Alternatively, FRCs in the T cell zone may also produce CXCL13 transcripts, but protein synthesis may be tightly regulated.

Notably, our data suggested that FRCs contribute to the maintenance of ECs. In addition to confirming FRC expression of VEGF-A[20], our analysis showed FRC-restricted expression of transcripts for other angiogenic and lymph-angiogenic molecules, including GREM1, VEGF-C and HGF[46], whereas FRCs, LECs and DNCs shared expression of ANGPTL4. Notably, BECs and LECs produced transcripts for the relevant receptors. Thus, it is likely that in addition to regulating the homeostasis of cells of hematopoietic origin, FRCs promote the survival and proliferation of ECs.

Little is known about the DNC niche. DNCs most closely resembled FRCs in terms of global gene expression and production of cytokines, chemokines and growth factors. DNC-specific probes showed enrichment for molecules involved in contractile function relative to those of FRCs, and cultured DNCs formed elongated networks that strongly contracted three-dimensional collagen matrices. *In vivo*, we found that ITGA7 was an effective surface marker for >50% of DNCs, subsequently identified as highly contractile cells that we called IAPs. Further studies are needed to elucidate any developmental relationship between IAPs and FRCs and whether IAP-ensheathed vessels demonstrate functional specialization.

Here we aimed to provide the first comparative transcriptome analysis of lymphoid organ stroma. Our data simultaneously supported and extended published findings while providing ready access to a comprehensive database of molecular determinants expressed by LNSCs. By comparison of stromal data with data gathered for hematopoietic cells, plausible webs of interaction became apparent. As an immunological resource, this expression-patterning analysis suggests that LNSCs are closely involved in many facets of immune regulation, structural support and stromal-cell homeostasis, which provides supportive data for many new avenues of study.

METHODS

Methods and any associated references are available in the online version of the paper at http://www.nature.com/natureimmunology/.

AUTHOR CONTRIBUTIONS
D.M. and A.L.F. designed the study, did and analyzed most experiments, and wrote the manuscript; S.J.T. designed and directed the study, analyzed and interpreted results, and wrote the manuscript; D.M. did primary analysis of the microarray data; V.L.-K., P.T., S.F.G., J.A., K.G.E. and K.K. did and analyzed individual experiments; and S.K.C., M.B.B., D.J.M., M.C.C. and M.E.H. contributed reagents and assisted with the analysis of individual experiments.

COMPETING FINANCIAL INTERESTS
The authors declare no competing financial interests.

1. Heng, T.S. & Painter, M.W. The Immunological Genome Project: networks of gene expression in immune cells. *Nat. Immunol.* **9**, 1091–1094 (2008).
2. Link, A. *et al.* Fibroblastic reticular cells in lymph nodes regulate the homeostasis of naive T cells. *Nat. Immunol.* **8**, 1255–1265 (2007).
3. Fletcher, A.L., Malhotra, D. & Turley, S.J. Lymph node stroma broaden the peripheral tolerance paradigm. *Trends Immunol.* **32**, 12–18 (2011).
4. Lee, J.W. *et al.* Peripheral antigen display by lymph node stroma promotes T cell tolerance to intestinal self. *Nat. Immunol.* **8**, 181–190 (2007).
5. Gardner, J.M. *et al.* Deletional tolerance mediated by extrathymic Aire-expressing cells. *Science* **321**, 843–847 (2008).
6. Fletcher, A.L. *et al.* Lymph node fibroblastic reticular cells directly present peripheral tissue antigen under steady-state and inflammatory conditions. *J. Exp. Med.* **207**, 689–697 (2010).
7. Cohen, J.N. *et al.* Lymph node-resident lymphatic endothelial cells mediate peripheral tolerance via Aire-independent direct antigen presentation. *J. Exp. Med.* **207**, 681–688 (2010).
8. Pham, T.H. *et al.* Lymphatic endothelial cell sphingosine kinase activity is required for lymphocyte egress and lymphatic patterning. *J. Exp. Med.* **207**, 17–27 (2010).
9. Sixt, M. *et al.* The conduit system transports soluble antigens from the afferent lymph to resident dendritic cells in the T cell area of the lymph node. *Immunity* **22**, 19–29 (2005).
10. Roozendaal, R., Mebius, R.E. & Kraal, G. The conduit system of the lymph node. *Int. Immunol.* **20**, 1483–1487 (2008).
11. Palframan, R.T. *et al.* Inflammatory chemokine transport and presentation in HEV: a remote control mechanism for monocyte recruitment to lymph nodes in inflamed tissues. *J. Exp. Med.* **194**, 1361–1373 (2001).
12. Itano, A.A. *et al.* Distinct dendritic cell populations sequentially present antigen to CD4 T cells and stimulate different aspects of cell-mediated immunity. *Immunity* **19**, 47–57 (2003).
13. Kalluri, R. & Zeisberg, M. Fibroblasts in cancer. *Nat. Rev. Cancer* **6**, 392–401 (2006).
14. Link, A. *et al.* Association of T-zone reticular networks and conduits with ectopic lymphoid tissues in mice and humans. *Am. J. Pathol.* **178**, 1662–1675 (2011).
15. Reich, M. *et al.* GenePattern 2.0. *Nat. Genet.* **38**, 500–501 (2006).
16. Huang, W.W., Sherman, B.T. & Lempicki, R.A. Systematic and integrative analysis of large gene lists using DAVID bioinformatics resources. *Nat. Protoc.* **4**, 44–57 (2009).
17. Mackay, F. & Leung, H. The role of the BAFF/APRIL system on T cell function. *Semin. Immunol.* **18**, 284–289 (2006).
18. Wei, S. *et al.* Functional overlap but differential expression of CSF-1 and IL-34 in their CSF-1 receptor-mediated regulation of myeloid cells. *J. Leukoc. Biol.* **88**, 495–505 (2010).
19. Watowich, S.S. & Liu, Y.J. Mechanisms regulating dendritic cell specification and development. *Immunol. Rev.* **238**, 76–92 (2010).
20. Chyou, S. *et al.* Fibroblast-type reticular stromal cells regulate the lymph node vasculature. *J. Immunol.* **181**, 3887–3896 (2008).
21. Liston, A. *et al.* Inhibition of CCR6 function reduces the severity of experimental autoimmune encephalomyelitis via effects on the priming phase of the immune response. *J. Immunol.* **182**, 3121–3130 (2009).
22. Kalamajski, S. & Oldberg, A. The role of small leucine-rich proteoglycans in collagen fibrillogenesis. *Matrix Biol.* **29**, 248–253 (2010).
23. Schvartz, I., Seger, D. & Shaltiel, S. Vitronectin. *Int. J. Biochem. Cell Biol.* **31**, 539–544 (1999).
24. van den Berg, T.K., van der Ende, M., Dopp, E.A., Kraal, G. & Dijkstra, C.D. Localization of beta 1 integrins and their extracellular ligands in human lymphoid tissues. *Am. J. Pathol.* **143**, 1098–1110 (1993).
25. Page-McCaw, A., Ewald, A.J. & Werb, Z. Matrix metalloproteinases and the regulation of tissue remodelling. *Nat. Rev. Mol. Cell Biol.* **8**, 221–233 (2007).
26. Chang, S.K., Gu, Z. & Brenner, M.B. Fibroblast-like synoviocytes in inflammatory arthritis pathology: the emerging role of cadherin-11. *Immunol. Rev.* **233**, 256–266 (2010).
27. Moll, R. *et al.* Endothelial and virgultar cell formations in the mammalian lymph node sinus: endothelial differentiation morphotypes characterized by a special kind of junction (complexus adhaerens). *Cell Tissue Res.* **335**, 109–141 (2009).
28. Yamamura, H., Hirano, N., Koyama, H., Nishizawa, Y. & Takahashi, K. Loss of smooth muscle calponin results in impaired blood vessel maturation in the tumor-host microenvironment. *Cancer Sci.* **98**, 757–763 (2007).
29. Mayer, U. *et al.* Absence of integrin α_7 causes a novel form of muscular dystrophy. *Nat. Genet.* **17**, 318–323 (1997).
30. Fitzgerald, K.A. *et al.* LPS-TLR4 signaling to IRF-3/7 and NF-κB involves the toll adapters TRAM and TRIF. *J. Exp. Med.* **198**, 1043–1055 (2003).
31. Khan, K.D., Lindwall, G., Maher, S.E. & Bothwell, A.L. Characterization of promoter elements of an interferon-inducible Ly-6E/A differentiation antigen, which is expressed on activated T cells and hematopoietic stem cells. *Mol. Cell. Biol.* **10**, 5150–5159 (1990).
32. Li, C. & Chan, Y.R. Lipocalin 2 regulation and its complex role in inflammation and cancer. *Cytokine* **56**, 435–441 (2011).
33. Fontaine, C. *et al.* The nuclear receptor Rev-erbα is a liver X receptor (LXR) target gene driving a negative feedback loop on select LXR-induced pathways in human macrophages. *Mol. Endocrinol.* **22**, 1797–1811 (2008).
34. Young, B.B., Gordon, M.K. & Birk, D.E. Expression of type XIV collagen in developing chicken tendons: association with assembly and growth of collagen fibrils. *Dev. Dyn.* **217**, 430–439 (2000).
35. Danielson, K.G. *et al.* Targeted disruption of decorin leads to abnormal collagen fibril morphology and skin fragility. *J. Cell Biol.* **136**, 729–743 (1997).
36. Bailey, A.J. Molecular mechanisms of ageing in connective tissues. *Mech. Ageing Dev.* **122**, 735–755 (2001).
37. Gilbert, D.L., Okano, T., Miyata, T. & Kim, S.W. Macromolecular diffusion through collagen membranes. *Int. J. Pharm.* **47**, 79–88 (1988).
38. Brennan, K. & Bowie, A.G. Activation of host pattern recognition receptors by viruses. *Curr. Opin. Microbiol.* **13**, 503–507 (2010).
39. Brass, A.L. *et al.* The IFITM proteins mediate cellular resistance to influenza A H1N1 virus, West Nile virus, and dengue virus. *Cell* **139**, 1243–1254 (2009).
40. Mueller, S.N. *et al.* Viral targeting of fibroblastic reticular cells contributes to immunosuppression and persistence during chronic infection. *Proc. Natl. Acad. Sci. USA* **104**, 15430–15435 (2007).
41. Tomei, A.A., Siegert, S., Britschgi, M.R., Luther, S.A. & Swartz, M.A. Fluid flow regulates stromal cell organization and CCL21 expression in a tissue-engineered lymph node microenvironment. *J. Immunol.* **183**, 4273–4283 (2009).
42. Lämmermann, T. & Sixt, M. The microanatomy of T-cell responses. *Immunol. Rev.* **221**, 26–43 (2008).
43. Chang, S.K. *et al.* Cadherin-11 regulates fibroblast inflammation. *Proc. Natl. Acad. Sci. USA* **108**, 8402–8407 (2011).
44. Kenins, L., Gill, J.W., Boyd, R.L., Hollander, G.A. & Wodnar-Filipowicz, A. Intrathymic expression of Flt3 ligand enhances thymic recovery after irradiation. *J. Exp. Med.* **205**, 523–531 (2008).
45. Roozendaal, R. *et al.* Conduits mediate transport of low-molecular-weight antigen to lymph node follicles. *Immunity* **30**, 264–276 (2009).
46. Mitola, S. *et al.* Gremlin is a novel agonist of the major proangiogenic receptor VEGFR2. *Blood* **116**, 3677–3680 (2010).

The complete list of authors is as follows:

Yan Zhou[10], Susan A Shinton[10], Richard R Hardy[10], Natalie A Bezman[11], Joseph C Sun[11], Charlie C Kim[11], Lewis L Lanier[11], Jennifer Miller[12], Brian Brown[12], Miriam Merad[12], Anne L Fletcher[13], Kutlu G Elpek[13], Angelique Bellemare-Pelletier[13], Deepali Malhotra[13,14], Shannon J Turley[13,15], Kavitha Narayan[16], Katelyn Sylvia[16], Joonsoo Kang[16], Roi Gazit[17], Brian Garrison[17], Derrick J Rossi[17], Vladimir Jojic[18], Daphne Koller[18], Radu Jianu[19], David Laidlaw[19], James Costello[20], Jim Collins[20], Nadia Cohen[21], Patrick Brennan[21], Michael B Brenner[21,22], Tal Shay[23], Aviv Regev[23], Francis Kim[24], Tata Nageswara Rao[24], Amy Wagers[24], Emmanuel L Gautier[12,25], Claudia Jakubzick[12,25], Gwendalyn J Randolph[12,25], Paul Monach[26], Adam J Best[27], Jamie Knell[27], Ananda Goldrath[27], Tracy Heng[15], Taras Kreslavsky[13], Michio Painter[15], Diane Mathis[15] & Christophe Benoist[15]

[10]Fox Chase Cancer Center, Philadelphia, Pennsylvania, USA. [11]Department of Microbiology & Immunology, University of California San Francisco, San Francisco, California, USA. [12]Icahn Medical Institute, Mount Sinai Hospital, New York, New York, USA. [13]Department of Cancer Immunology and AIDS, Dana-Farber Cancer Institute, Boston, Massachusetts, USA. [14]Division of Medical Sciences, Harvard Medical School, Boston, Massachusetts, USA. [15]Department of Microbiology and Immunobiology, Harvard Medical School, Boston, Massachusetts, USA. [16]University of Massachusetts Medical School, Worcester, Massachusetts, USA. [17]Immune Disease Institute, Children's Hospital, Boston, Massachusetts, USA. [18]Computer Science Department, Stanford University, Stanford, California, USA. [19]Computer Science Department, Brown University, Providence, Rhode Island, USA. [20]Department of Biomedical Engineering, Howard Hughes Medical Institute, Boston University, Boston, Massachusetts, USA. [21]Division of Rheumatology, Immunology and Allergy, Brigham and Women's Hospital, Boston, Massachusetts, USA. [22]Department of Medicine, Harvard Medical School, Boston, Massachusetts, USA. [23]Broad Institute, Cambridge, Massachusetts, USA. [24]Joslin Diabetes Center, Boston, Massachusetts, USA. [25]Department of Pathology & Immunology, Washington University, St. Louis, Missouri, USA. [26]Department of Medicine, Boston University, Boston, Massachusetts, USA. [27]Division of Biological Sciences, University of California San Diego, La Jolla, California, USA.

ONLINE METHODS

Mice. According to standard operating protocols of the ImmGen Project, all mice used were 6-week-old male C57BL/6 mice from the Jackson Laboratory, shipped 1 week before use and maintained under specific pathogen–free conditions. OT-I mice deficient in recombination-activating gene 2 (Taconic) were bred at the Dana-Farber Cancer Institute. Mice were cared for under institutional and US National Institutes of Health guidelines. Experiments received approval from the Research Animal Care subcommittee at the Dana-Farber Cancer Institute.

Induction of inflammation. OT-I T cells (1.5×10^6) were transferred intravenously to C57BL/6 mice. Then, 18 h later, mice received intravenous injection of 30 µg lipopolysaccharide from *E. coli* (serotype 0127:B8; L3129; Sigma-Aldrich) and 500 µg ovalbumin (A5503; Sigma-Aldrich). SLNs were collected 12 h after injection for sorting of FRCs, LECs and BECs for microarray analysis. SLNs were collected 18 h after injection for analysis of the expression of MHC class II and LCN2 protein.

Antibodies and conjugates. The following antibodies and stains were used: anti-CD45 (30-F11; Biolegend), anti-Ter119 (Ter119; Biolegend), anti-CD31 (MEC13.3; Biolegend), anti-gp38 (8.1.1; purified in-house from a hybridoma from the Developmental Studies Hybridoma Bank), anti-CD140a (APA5; eBioscience), anti-MAdCAM-1 (MECA-367; eBioscience), anti-cadherin-11 (13C2 and isotype-matched control antibody MOPC21; M.B.), anti–mouse I-A and I-E (M5/114.15.2; Biolegend), anti–mouse CD44 (IM7; eBioscience), polyclonal anti–collagen VI (ab6588; Abcam), polyclonal anti–collagen XIV (M. Koch), anti-vitronectin (ab28023; Abcam), ER-TR7 (ab51824; Abcam), anti–α-smooth muscle actin (1A4; Sigma-Aldrich), anti-ITGA7-FITC (3349908; R&D Systems), anti-CNN1 (EP7984; Epitomics), polyclonal anti-fibromodulin (batch LF-150; L. Fisher), polyclonal–anti-mouse-decorin (batch LF-113; L. Fisher[47]), polyclonal-anti-mouse-biglycan (batch LF-159; L. Fisher[47]), polyclonal-anti-desmin (ab15200; Abcam), anti-pNAd–biotin (MECA-79; Biolegend), anti-LYVE-1–Alexa Fluor 488 (ALY7; eBioscience), polyclonal anti-LCN2 (AF1857; R&D Systems), anti–hamster immunoglobulin G (IgG)–Alexa Fluor 488 (A-21110; Invitrogen), anti–rat IgG–Alexa Fluor 647 (A-21247; Invitrogen), anti–rabbit IgG–Alexa Fluor 488 (A-11034; Invitrogen), anti-rabbit IgG–Alexa Fluor 647 (A-31573; Invitrogen), anti–rabbit IgG–Alexa Fluor 555 (A-31572; Invitrogen), anti–goat IgG–Alexa Fluor 488 (A-11055; Invitrogen), anti–goat IgG–biotin (A-10518; Invitrogen), anti–mouse IgG1–biotin (550331; BD), anti–mouse IgG–Alexa Fluor 488 (A-11029; Invitrogen), polyclonal anti–mouse ADAM10 (AB946; R&D), DAPI (D3571; Invitrogen), TRITC-phalloidin (R415, Invitrogen), streptavidin–Alexa Fluor 555 (S-32355; Invitrogen) and streptavidin–Alexa Fluor A488 (S-32354; Invitrogen).

Cell enrichment and sorting. Cells were prepared according to standard operating protocols of the ImmGen Project. Skin-draining lymph nodes (inguinal, axillary and brachial) and mesenteric lymph nodes were isolated from C57BL/6 mice ($n = 10–30$), then were digested, enriched for CD45⁻ stroma and sorted as described[6,48]. For skin fibroblasts, mouse ears ($n = 5$ mice per group) were placed in ice cold RPMI medium, 2% FBS, then were split and sliced with a razor blade and digested as described[6]. Red blood cells were lysed (140 mM NH₄Cl and 17 mM Tris-base, pH 7.4) and cells were stained and sorted (single round of sorting) directly into TRIzol with a FACSAria (100-µm nozzle; 20 psi). Dead cells were excluded with propidium iodide (5 ng/ml). Purity was assessed by sorting of cells into flow cytometry buffer (2% FBS, 2 mM EDTA and PBS) followed by immediate analysis of samples with a FACSAria. RNA was isolated as described[49].

Microarray hybridization and data normalization. Isolated RNA was amplified and prepared for hybridization to the Affymetrix MoGene 1.0 ST array with the GeneChip Whole Transcript (WT) Sense Target Labeling Assay in accordance with manufacturer's instructions. Raw data were normalized with the robust multichip average algorithm in the ExpressionFileCreator module of the GenePattern genomic analysis platform.

Expression value probabilities. Thresholds for likelihood of positive gene expression were determined from the distribution of expression across the microarrays. Because the ST1.0 arrays do not contain reliable negative controls, a Gaussian mixture model was used to determine probabilistic thresholds of expression, an approach initially confirmed by comparison of parallel data sets obtained from the same RNA from B lymphocytes and T lymphocytes[49]. Probabilities of components in the model were combined to arrive at a single probability of expression. Thresholds were calculated for each sample, and the distribution of cutoffs was examined to determine whether a single value could be applied to all samples from the ImmGen Project. An expression value of 120 after normalization, which corresponds to a 95% probability of expression, was used as the standard cutoff for gene expression for most populations from the ImmGen Project.

Population distance measurements. PCA was done on expressed probes with the ImmGen Population PCA Plot module for GenePattern. PCA simplifies complex, multidimensional data into principal components. Each principal component is uncorrelated with earlier principal components to account for maximal variability among populations. This module identified and used the 15% of probes with the greatest difference in expression across populations for PCA. PCA used $\log_2$-transformed and row- and column-normalized data. The 15% most variable probes were identified in an unsupervised manner: for all expressed probes (EV > 120 for any subset), the module uses replicate values to compute the standard deviation within each population and averages these values to generate a single standard deviation value that reflects variability within each cell type (s.d. within), and uses mean expression values to calculate a single standard deviation across all cell populations (s.d. across). Probes were ranked according to the following ratio: s.d. across/s.d. within. Probes with the highest ratios were determined to be the most variable, and the top 15% of these were used. The first three principal components were used as coordinate-axes onto which samples were projected. Pearson correlation coefficients and Euclidean distances were calculated with the same probes. Data was $\log_2$ transformed and row standardized. Correlation and distance values were computed with R software (the R project for statistical computing). Heat maps were generated with the HeatMapImage module of GenePattern.

Hierarchical clustering analysis. With the Multiplot module of GenePattern, probes with different expression were identified (FC > 2 in at least one pair-wise population comparison; EV > 120 for at least one population), then clustered (Pearson's correlation and average linkage) with the HierarchicalClustering module of GenePattern. Data were $\log_2$ transformed, row centered and row normalized, then visualized with the HierarchicalClusteringViewer module of GenePattern.

Stromal gene-signature determination (delta-score analysis). The ImmGen Project Delta Score module for GenePattern was used to identify stromal cell–specific signatures in a pair-wise manner. For two populations, *a* and *b*, effective differences in expression were defined as follows:

$$\delta(a,b) = \log_2\left(\frac{\mu_a}{\mu_b}\right) - \left(\sigma_a + \sigma_b\right)^2$$

where μ and σ are the geometric mean and geometric standard deviation, respectively, of the two populations. The ratio in the first term represents the FC between the class means of *a* and *b*. This value was $\log_2$ transformed (so a power of 2 corresponds to FC). FC values are penalized for noise within replicates by subtraction of the square of the sum of the geometric standard deviation of both populations. The resulting delta score (δ) reflects noise-adjusted differences between the two populations. A δ of 1 corresponds to an adjusted FC of ≥2, a δ of 2 corresponds to an adjusted FC of ≥4 and so on. Lists of probes with differences in expression were combined for subsequent analysis by Excel.

Probes subsequently identified as having significantly different expression ($P < 0.05$; *t*-test) were used (Multiplot module of GenePattern).

Analysis of functional enrichment in gene signatures. Population-specific lists were analyzed with the Functional Annotation Tool of DAVID[16]. Lists were uploaded as official gene symbols for *Mus musculus*. The background was set to the MoGene-1_0-st-v-1 chip. In the Pathways option, the KEGG_Pathway chart was selected. Count requirements for genes were set as 0 and

the EASE score was set as 1. Top-ranked or biologically significant 'hits' are presented with *P* values corrected by the multiple-hypothesis test (Benjamini procedure).

Other general microarray analysis details. For bar graphs and heat maps of genes with multiple probes, a single representative probe (the probe closest to the mean in Euclidean distance) was used for visualization.

Immunofluorescence microscopy. Lymph nodes were snap-frozen in optimum cutting temperature compound. For staining of ITGA7, CNN1 and LCN2, lymph nodes were fixed for 4 h in 4% paraformaldehyde and then overnight in 30% sucrose before being frozen. Sections 7.5 μm in thickness were cut and blocked with FcR block (2.4G2) and 2% BSA before being stained with primary and secondary antibodies. For staining of fibromodulin, sections were pretreated for 1 h at 37 °C with chondroitinase ABC (Sigma). For staining of cadherin-11 on cultured FRCs, 2.5×10^4 cells were plated overnight on coverslips coated with fibronectin (33016-015; Invitrogen). Cells were blocked as described above and incubated with primary antibodies. Cells were fixed with 4% PFA, permeablized with 0.2% Triton-X-100 (T-9284; Sigma) and then incubated with secondary conjugates. Sections were visualized with a laser-scanning confocal microscope (Leica SP5X) and analyzed with ImageJ (NIH) and Adobe Photoshop CS.

Electron microscopy. Popliteal lymph nodes were prepared and analyzed as described[50].

Flow cytometry. Lymph nodes were digested and stained as described[6]. For staining of cadherin-11, cells were prepared and stained in EDTA-free HEPES-buffered saline with 2% FBS and 1 mM $CaCl_2$. Samples were acquired on a FACSCalibur or FACSAria (BD Biosciences) and analyzed with FlowJo v.8.7.3 software.

Contraction assay. C2C12 myoblasts and NIH3T3 fibroblasts were cultured until 70% confluent. FRCs from SLNs were cultured as described[6]. Cells (5×10^5) were suspended in 500 μl gel (1 mg/ml rat tail collagen I (BD Biosciences) in αMEM) and seeded into tubular constructs. Images were obtained with a Nikon camera and analyzed with ImageJ, and contraction was measured as the width of collagen matrix divided by total tube width.

RT-PCR. RNA extraction, cDNA preparation and PCR cycling conditions have all been described[6]. Primers (Integrated DNA Technologies) were as follows: CXCL13F, TGGCCAGCTGCCTCTCTC; and CXCL13R, TTGAAATCACT CCAGAACACCTACA.

Statistics. Multiplot (GenePattern) was used for computation of *t*-test *P* values. For functional enrichment in gene lists, *P* values were corrected for multiple hypothesis testing with the Benjamini option of the DAVID Functional Annotation Tool. *P* values for the χ^2 test with Yates' correction were computed with GraphPad Prism 5. False-discovery-rate-adjusted *P* values were calculated with the ComparativeMarkerSelection module of GenePattern, which uses the Benjamini and Hochberg procedure.

47. Fisher, L.W., Stubbs, J.T. III & Young, M.F. Antisera and cDNA probes to human and certain animal model bone matrix noncollagenous proteins. *Acta Orthop. Scand. Suppl.* **266**, 61–65 (1995).
48. Fletcher, A. *et al.* Reproducible isolation of lymph node stromal cells reveals site-dependent differences in fibroblastic reticular cells. *Front. Immunol.* **2**, 35 (2011).
49. Painter, M.W., Davis, S., Hardy, R.R., Mathis, D. & Benoist, C. Transcriptomes of the B and T lineages compared by multiplatform microarray profiling. *J. Immunol.* **186**, 3047–3057 (2011).
50. Gonzalez, S.F. *et al.* Capture of influenza by medullary dendritic cells via SIGN-R1 is essential for humoral immunity in draining lymph nodes. *Nat. Immunol.* **11**, 427–434 (2010).